inorganics

MDPI

Article

Optimization of Electrochemical Performance of $LiFePO_4$/C by Indium Doping and High Temperature Annealing

Ajay Kumar [1], Parisa Bashiri [1], Balaji P. Mandal [1], Kulwinder S. Dhindsa [1], Khadije Bazzi [1], Ambesh Dixit [2], Maryam Nazri [1], Zhixian Zhou [1], Vijayendra K. Garg [3], Aderbal C. Oliveira [3], Prem P. Vaishnava [4], Vaman M. Naik [5], Gholam-Abbas Nazri [1,6] and Ratna Naik [1,*]

1 Department of Physics and Astronomy, Wayne State University, Detroit, MI 48202, USA; ajay.kumar3@wayne.edu (A.K.); parisa.bashiri@wayne.edu (P.B.); bpmandal80@gmail.com (B.P.M.); ee3087@wayne.edu (K.S.D.); eb2920@wayne.edu (K.B.); maryam.nazri@wayne.edu (M.N.); dw0795@wayne.edu (Z.Z.); nazri@wayne.edu (G.-A.Z.)
2 Indian Institute of Technology, Jodhpur 342011, India; adixit2@gmail.com
3 Universidade de Brasilia, Instituto de Fisica, Brasilia, DF 70919-970, Brazil; vijgarg@gmail.com (V.K.G.); aderbal47@gmail.com (A.C.O.)
4 Department of Physics, Kettering University, Flint, MI 48504, USA; pvaishna@kettering.edu
5 Department of Natural Sciences, University of Michigan-Dearborn, Dearborn, MI 48128, USA; vmnaik@umich.edu
6 Electrical and Computer Engineering, Wayne State University, Detroit, MI 48202, USA
* Correspondence: rnaik@wayne.edu; Tel.: +1-313-577-2818

Received: 11 August 2017; Accepted: 2 October 2017; Published: 10 October 2017

Abstract: We have prepared nano-structured In-doped (1 mol %) $LiFePO_4$/C samples by sol–gel method followed by a selective high temperature (600 and 700 °C) annealing in a reducing environment of flowing Ar/H_2 atmosphere. The crystal structure, particle size, morphology, and magnetic properties of nano-composites were characterized by X-ray diffraction (XRD), scanning electron microsopy (SEM), transmission electron microscopy (TEM), and ^{57}Fe Mössbauer spectroscopy. The Rietveld refinement of XRD patterns of the nano-composites were indexed to the olivine crystal structure of $LiFePO_4$ with space group *Pnma*, showing minor impurities of Fe_2P and Li_3PO_4 due to decomposition of $LiFePO_4$. We found that the doping of In in $LiFePO_4$/C nanocomposites affects the amount of decomposed products, when compared to the un-doped ones treated under similar conditions. An optimum amount of Fe_2P present in the In-doped samples enhances the electronic conductivity to achieve a much improved electrochemical performance. The galvanostatic charge/discharge curves show a significant improvement in the electrochemical performance of 700 °C annealed In-doped-$LiFePO_4$/C sample with a discharge capacity of 142 mAh·g^{-1} at 1 C rate, better rate capability (~128 mAh·g^{-1} at 10 C rate, ~75% of the theoretical capacity) and excellent cyclic stability (96% retention after 250 cycles) compared to other samples. This enhancement in electrochemical performance is consistent with the results of our electrochemical impedance spectroscopy measurements showing decreased charge-transfer resistance and high exchange current density.

Keywords: Lithium iron phosphate; conductive Fe_2P; indium doping

1. Introduction

$LiFePO_4$ has become one of the most viable commercial cathode materials after the ground breaking work of Padhi et al. [1]. This material has received an extensive attention due to its high thermal and electrochemical safety, lower cost compared to mixed oxide cathode materials, low toxicity,

stable voltage range even at overcharge condition, and long cycle life. However, the poor electronic conductivity and slow diffusion of lithium ion in bulk $LiFePO_4$ have been major challenges requiring new electrode material engineering. To improve electronic conductivity and reduce lithium ion diffusion length, many approaches, such as reducing the particle size to nanoscale [2–5], coating the particles with conductive carbon [6–12], and doping $LiFePO_4$ with various cations [13–20] have been proposed. In addition, $LiFePO_4$ decomposes above 700 °C leading to in-situ formation of conductive iron phosphides (Fe_2P, FeP, Fe_3P), and compounds with superior lithium-ion diffusion coefficients, such as, Li_3PO_4 and $Li_2FeP_2O_7$ [21–26]. Although initial formation of conductive iron phosphides at the grain boundaries improves electrochemical performance, these phases are not electrochemically active and excessive decomposition of $LiFePO_4$ reduces the active material leading to reduced specific capacity of the sample. Therefore, careful annealing temperature and addition of proper amount of dopants that reduce the decomposition of active material is crucial for preparation of high performance $LiFePO_4$ cathode materials. In our previous work [27], we studied the formation Fe_2P and Li_3PO_4 by the decomposition of $LiFePO_4$/C as a function of annealing temperature between 600–900 °C in a reducing environment and found that the amount of Fe_2P increases very steeply from 5 to 38 wt % with the annealing temperature. Li_3PO_4 may contribute to the high ionic conduction at the electrode/electrolyte interface when preferentially deposited on the surface at the grain boundaries [28]. The presence of conductive Fe_2P significantly improved the electronic conductivity of the samples which varied from 2×10^{-3} S·cm^{-1} (600 °C) to 2×10^{-1} S·cm^{-1} (900 °C). Of all the samples studied, the $LiFePO_4$/C sample calcined at 700 °C which consists of 14 wt % of Fe_2P exhibited a better electrochemical performance with a discharge capacity of ~136 mAh·g^{-1} at 1 C, ~121 mAh·g^{-1} at 10 C (70% of the theoretical capacity of $LiFePO_4$), and excellent cycleability. The observed steep decrease in the discharge capacity of samples annealed at higher temperatures was attributed to the increased amount of inactive decomposed products in the electrode. Hence, our previous work suggests that the synthesis environment can be controlled to optimize the amount of Fe_2P to obtaining the best discharge capacity of $LiFePO_4$/C nanocomposites.

In addition, cation doping at Li and Fe sites in $LiFePO_4$ have been investigated by several researchers [13–20] to improve the electrochemical properties of $LiFePO_4$. Substitution of Mg, Al, Na at Li sites [14,15,19] have been shown to improve the overall electrochemical properties of $LiFePO_4$. Theoretical calculations by Islam et al. [20] have suggested, on energetic grounds, that $LiFePO_4$, is favorable for divalent dopants (e.g., Mg, Mn, Co), but not tolerant to aliovalent doping (e.g., Nd, La, In) on either Li (M1) or Fe (M2) sites. Nevertheless, a few experimental studies have investigated the effects of substituting aliovalent ions, such as Gd, Nd, La, at Fe sites in $LiFePO_4$ [16–18]. For example, 1% La-doped $LiFePO_4$/C sample showed the best electrochemical behavior with a discharge capacity of 156 mAh·g^{-1} at a rate of 0.2 C [18]. However, there have been no experimental studies available in the literature to see the effect of In-doping in $LiFePO_4$. There are multiple beneficial effects expected with In-doping. The redox potential of indium in nonaqueous electrolyte has shown that In remains in 3-oxidation state (In^{III}) at voltages above 1.5 V vs. lithium. In addition, indium oxide has superior electronic conductivity compared to the $LiFePO_4$ that may lead to an improved electronic conductivity, particularly when it resides on the surface of the sample. On the other hand, if some of the iron sites are occupied by indium ions, it may increase the concentration of charge carrier in the sample as indium has a high thermodynamic tendency to remain as In^{III} cation, while Fe in the original $LiFePO_4$ material is at Fe^{II} state. Furthermore, the indium ion is a more polarizable, softer and diffuse ion than the hard sphere Fe^{III}. Therefore, Indium doping may reduce ionic lattice energy and energy barrier for Li-ion hopping between available sites.

In this work, we have studied the effect of In (1 mol %)-doping on the formation of Fe_2P due to decomposition of $LiFePO_4$/C nanocomposites when annealed at two different temperatures of 600 and 700 °C in a reducing environment. We find that the In-doped-$LiFePO_4$/C sample annealed at 700 °C which consists of 11 wt % of Fe_2P showed an improved discharge capacity (142 mAh·g^{-1} at 1 C rate), better rate capability at higher rates (~128 mAh·g^{-1} at 10 C rate, ~75% of the theoretical capacity) and excellent cyclic stability compared to that of un-doped sample annealed

under similar conditions. By combining In-doping with high temperature (700 ± 50 °C) annealing, the electrochemical performance of $LiFePO_4$/C can be further improved by optimizing the amount of Fe_2P in the nanocomposites for good electronic conductivity without sacrificing the active material.

2. Results and Discussion

2.1. X-ray Diffraction

The In-doped-$LiFePO_4$/C samples were analyzed by XRD to verify both the crystallinity and phase purity. Their XRD patterns (Figure 1) were indexed to an orthorhombic $LiFePO_4$ phase with space group *Pnma*, according to the standard pattern of JCPDF 83-2092, indicating that an olivine-type structure is well maintained upon doping with 1 mol % of In. We do notice the presence of minor impurity phases that are indexed to iron phosphide (Fe_2P) and lithium phosphate (Li_3PO_4), which are formed, particularly, in In-LFP-700 sample. We have performed Rietveld analysis of XRD patterns using GSAS (General Structure Analysis System, Los Alamos National Laboratory Report LAUR 86-748 (2000)), software implemented with EXPGUI interface, to estimate the amount of Fe_2P and Li_3PO_4 in In-LFP-600 and In-LFP-700 samples (Figure 1), and the estimated amounts are listed in Table 1. For comparison, we have also including the data for LFP-600 and LFP-700 samples from our previous study [27]. The threshold temperature for forming Fe_2P from the decomposition of $LiFePO_4$/C appears to be around 700 °C for both un-doped and doped samples. It is interesting to note the amount of Fe_2P formed is less in In-LFP-700 compared to LFP-700 sample. In-doping seems to reduce the formation of Fe_2P or the rate of decomposition of $LiFePO_4$/C at 700 °C. As Fe_2P is conducting, it affects the conductivity of the In-doped-$LiFePO_4$/C and hence its electrochemical properties. The reduction of Fe_2P with in In-doping in In-LFP-700, as indicated by XRD Rietveld analysis, is also confirmed by Mössbauer spectroscopy measurement, as discussed in a later section. The effect of In-doping on the crystallite size was also investigated using Rietveld fitting (GSAS software package) of the XRD patterns. The In-doped samples seem to have slightly smaller crystallite size compared to un-doped samples.

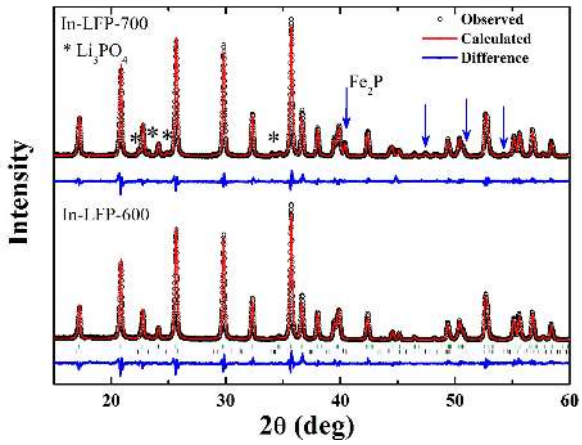

Figure 1. XRD patterns and Rietveld refinement of In-LFP-600 and In-LFP-700 samples.

Table 1. Values of $LiFePO_4$, Fe_2P and Li_3PO_4 estimated from Rietveld analysis of XRD patterns.

Sample	$LiFePO_4$ (wt %)	* Fe_2P (wt %)	Li_3PO_4 (wt %)	Crystallite Size (nm)
LFP-600 *	97.1	0	2.9	99
In-LFP-600	98.6	0	1.4	97
LFP-700 *	93.2	3.6	3.2	102
In-LFP-700	94.6	2.2	3.2	94

* see reference [27].

2.2. Electrical Conductivity

The room temperature electrical conductivity was measured for the samples using Van der Pauw method. The electronic conductivity for the LFP-600, In-LFP-600, LFP-700 and In-LFP-700 are 2×10^{-3}, 8×10^{-3}, 8×10^{-2} and 1×10^{-2} S·cm^{-1}, respectively. These results indicate that electronic conductivity of un-doped samples increases with the annealing temperature which is attributed to the formation of conductive Fe_2P phase at higher temperatures. We will show from our Mössbauer data analysis that the electrical conductivity correlates with the amount of Fe_2P (crystalline or sub-nanocrystalline) present in these samples [27].

2.3. Morphology and Microstructure

The morphology of the In-LFP-600 and In-LFP-700 samples was analyzed by SEM and they are shown in Figure 2a,b. The samples show a uniform distribution of nearly spherical particles with some agglomerated particles very similar to the un-doped samples [27], and 1 mol % In-doping does not affect the morphology significantly. This could be due to the fact that once the particles are carbon coated, the particle growth and the formation of aggregates are suppressed. In addition, the presence of carbon prevents the oxidation of Fe^{2+} to Fe^{3+}. Thus, the addition of the surfactant, lauric acid, is believed to play a crucial role in controlling the particle size and morphology of samples. We also investigated the particle size distribution using TEM as shown in Figure 2c,d for In-LFP-600 and In-LFP-700 samples. Again, the size distribution is very similar to the corresponding un-doped samples (~80–100 nm), with a rough morphology due to decomposition of $LiFePO_4$ into Fe_2P and Li_3PO_4. Our previous work [27] also showed that the particle surface of un-doped samples (for example, LFP-700) reveals sub-nano (2–4 nm) regions of the decomposed products, which may not be detected by XRD. The TEM the results are consistent with the average particle size calculated using XRD patterns.

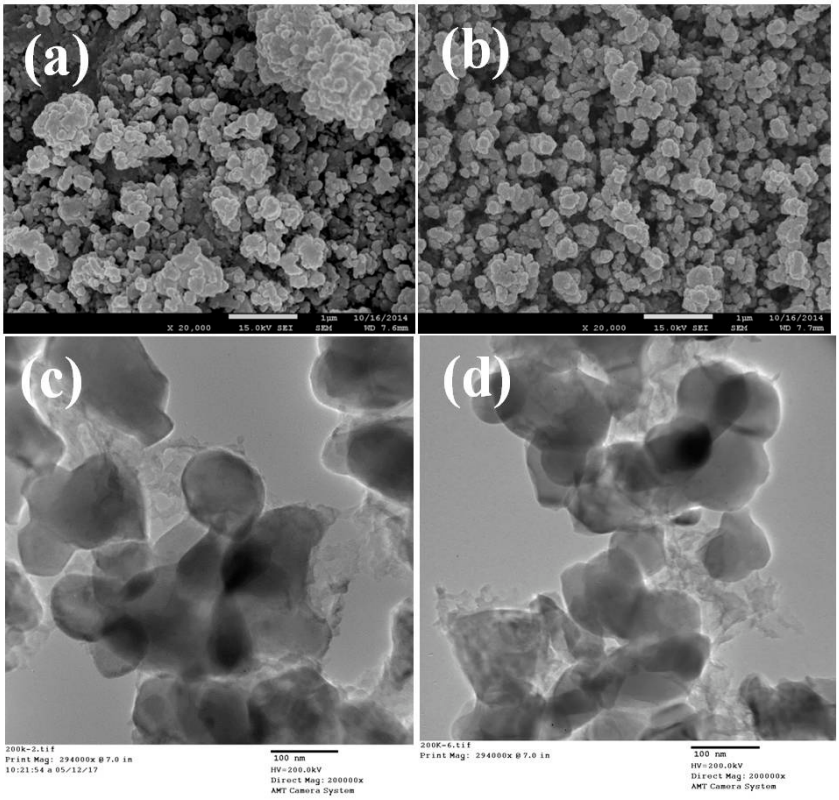

Figure 2. SEM images of (**a**) In-LFP-600 and (**b**) In-LFP-700 samples and their corresponding TEM images (**c**,**d**). The scale bars in (**a**,**b**) represent 1 μm and 100 nm in (**c**,**d**).

2.4. X-ray Photoelectron Spectroscopy

X-ray photoelectron spectroscopy allows us to access the local environment of atoms and their oxidation states. The technique, therefore, is used to differentiate between Fe^{3+} and Fe^{2+}. The Fe elemental XPS spectra of In-LFP-600 and In-LFP-700 samples are shown in Figure 3. All the spectra were fitted with three peaks, two at 710 and 714.5 eV are due to Fe^{2+} ions in $LiFePO_4$ and the third one at 712 eV due to Fe^{3+} originate mainly from $FePO_4$ and/or Fe_2P in agreement with the literature values [29,30]. The amount of ferric iron in In-LFP-600 was determined to be lower (~10%) compared to In-LFP-700 (~13%) sample, which is consistent with the Mössbauer spectroscopy measurements as described in Section 2.5.

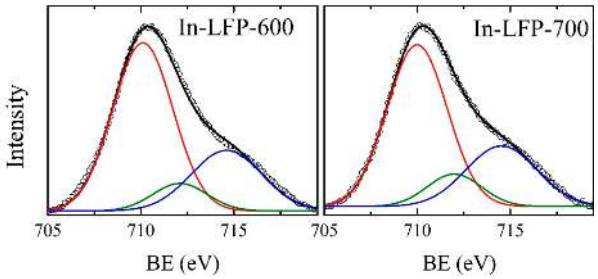

Figure 3. XPS spectra of Fe of In-LFP-600 and In-LFP-700 samples.

2.5. ^{57}Fe Mossbauer Spectroscopy

The room temperature ^{57}Fe Mössbauer spectra for the In-LFP-600 and In-LFP-700 samples are shown in Figure 4 to confirm the presence of Fe_2P. A summary of the Mössbauer parameters are given in Table 2. The ^{57}Fe Mössbauer spectrum of $LiFePO_4$ with Fe_2P consists of three quadrupole doublets. The dominant symmetric doublet with an isomer shift (IS) of 1.22 mm/s and quadrupole splitting (QS) of 2.97 mm/s arises from the high spin Fe^{2+} configuration of the 3*d* electrons and the distorted environment at the Fe atom in $LiFePO_4$ [31,32]. The other two doublets in the Mössbauer spectrum arise from two different favorable sites for Fe^{3+}, namely, tetrahedral with four nearest neighbor P atoms (3*f* site) and pyramidal with five nearest neighbor P atoms (3*g* site) in the structure of Fe_2P [31]. The second doublet with an IS of 0.61 mm/s and a QS of 0.43 mm/s is assigned to Fe^{3+} occupying 3*f* site and the third doublet with an IS of 0.19 mm/s and a QS of 0.1 mm/s is assigned to Fe^{3+} occupying 3*g* site in Fe_2P in the samples annealed at 700 °C [32]. The amount of Fe^{2+} and Fe^{3+} have been estimated using relative area under the corresponding peaks in the Mössbauer spectra. Table 2 lists the percentage of Fe^{2+} and Fe^{3+} phases and Table 3 lists the corresponding mol % and wt % of $LiFePO_4$, Fe_2P and Li_3PO_4 calculated using Equation (1). We have also listed the data for un-doped samples, LFP-600 and LFP-700, for a comparison.

$$6LiFePO_4 + 8C \rightarrow 3Fe_2P + 2\ Li_3PO_4 + P\uparrow + 8CO_2\uparrow \quad (1)$$

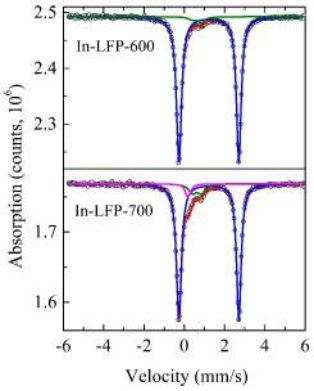

Figure 4. Mössbauer spectra of In-LFP-600 and In-LFP-700 samples measured at room temperature.

Table 2. Room temperature Mossbauer parameters of In-doped $LiFePO_4$/C samples annealed at 600 °C and 700 °C.

Sample	Doublet 1			Doublet 2			Doublet 3			Total
	IS	QS	%	IS	QS	%	IS	QS	%	Fe_2P (%)
In-LFP-600	1.22	2.97	92.2	0.61	0.43	7.8	-	-	-	7.8
In-LFP-700	1.22	2.97	86.7	0.61	0.43	8.7	0.19	0.10	4.6	13.3
		Fe^{2+}			Fe(I) site of Fe_2P			Fe(II) site of Fe_2P		

We note that the total amount of Fe_2P determined by Mössbauer spectroscopy do not agree with the estimated values by Rietveld refinement of the XRD data (Table 1). As discussed in our earlier work [27], this is due to presence of amorphous or sub-nanoregions of Fe_2P and Li_3PO_4.

Table 3. Percentage of $LiFePO_4$, Fe_2P and Li_3PO_4 in LFP and In-LFP samples annealed at 600 °C and 700 °C deduced from Mössbauer measurements.

Sample	$LiFePO_4$		Fe_2P		Li_3PO_4		Capacity ($mAh{\cdot}g^{-1}$)	
	mol %	wt %	mol %	wt %	mol %	wt %	Expected [a]	Measured at 1 C [b]
LFP-600 *	91.5	92.8	5.1	4.7	3.4	2.5	158	120
In-LFP-600	87.7	89.5	7.4	6.8	4.9	3.7	152	134
LFP-700 *	75.8	78.9	14.5	13.7	9.7	7.4	134	136
In-LFP-700	79.6	82.4	12.2	11.4	8.2	6.2	140	142

[a] 170 $mAh{\cdot}g^{-1}$ × wt % of $LiFePO_4$; [b] ± % due to uncertainty in mass determination; * see reference [27].

2.6. Electrochemical Measurements

Galvanostatic charge/discharge curves of the coin cells prepared with un-doped and indium doped $LiFePO_4$/C cathodes were measured between 2.2–4.2 V versus lithium at different rates. Charge/discharge curves for In-LFP-600 and In-LFP-700 samples at 1 C are depicted in Figure 5. Typical two-phase nature of the lithium extraction and insertion reactions between $LiFePO_4$ and $FePO_4$ is implied by the flat nature of the charge-discharge potential curves around ~3.4 V [33]. The steep rise and fall in the profiles at the large specific capacity values refer to the charge transfer activation and concentration polarizations with contribution from limited miscibility between the $LiFePO_4$ and $FePO_4$. The expected capacities calculated by taking into account the amount of observed Fe_2P and Li_3PO_4 masses from the Mössbauer measurements, and the measured capacities for the samples are listed in Table 3. The data clearly shows that the expected (~158 $mAh{\cdot}g^{-1}$ and 152 $mAh{\cdot}g^{-1}$) and measured capacities (~120 $mAh{\cdot}g^{-1}$ and ~136 $mAh{\cdot}g^{-1}$) for LFP-600 and In-LFP-600 differ significantly, although the latter sample shows significant improvement due to improved electronic conductivity. At higher annealing temperature of 700 °C, the expected and measured capacities are very close to each other, and the capacity of In-LFP-700 (142 $mAh{\cdot}g^{-1}$) is larger than the corresponding un-doped sample. We observe that at both the annealing temperatures, the measured capacity increases upon adding the indium dopant.

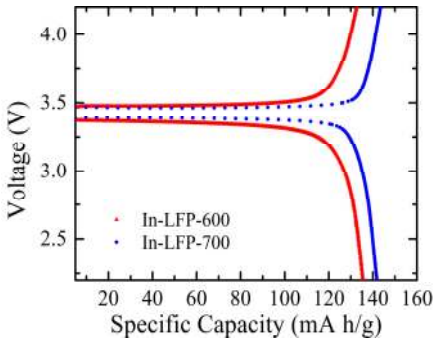

Figure 5. Charge/discharge profiles of In-LFP-600 and In-LFP-700 samples measured at 1 C rate.

The capacity of the samples at various charge/discharge rates are shown in Figure 6, including the data for un-doped LFP-600 and LFP-700 samples for a comparison. At higher rate, for example at 10 C, the supply of electrons from the interface electrochemical reaction becomes a problem leading to a lower specific capacity for un-doped sample annealed at 600 °C. However, addition of In increases its capacity because of its enhanced electronic conductivity. As seen in Figure 6, even at a high charge/discharge of 10 C the capacity of un-doped $LiFePO_4/C$ annealed at 600 °C increases from 84 $mAh{\cdot}g^{-1}$ to 114 $mAh{\cdot}g^{-1}$ upon doping with In. When the doped sample is annealed at 700 °C, the performance of the In-LFP-700 improves slightly at all rates, and at 10C rate it approached 128 $mAh{\cdot}g^{-1}$ (75% of the theoretical capacity). The inset in Figure 6 shows the cycling performance of the doped and un-doped samples annealed at 700 °C for 250 cycles. Clearly, In-LFP-700 shows better charge/discharge stability compared to the corresponding un-doped sample, and even after 250 cycles at 10 C rate the sample retains 96% of its initial capacity. Our results suggest that a combination of In-doping and annealing at high temperatures (700 ± 50 °C), the electrochemical performance of $LiFePO_4/C$ can be further improved by optimizing the amount of Fe_2P for good electronic conductivity without sacrificing the active material.

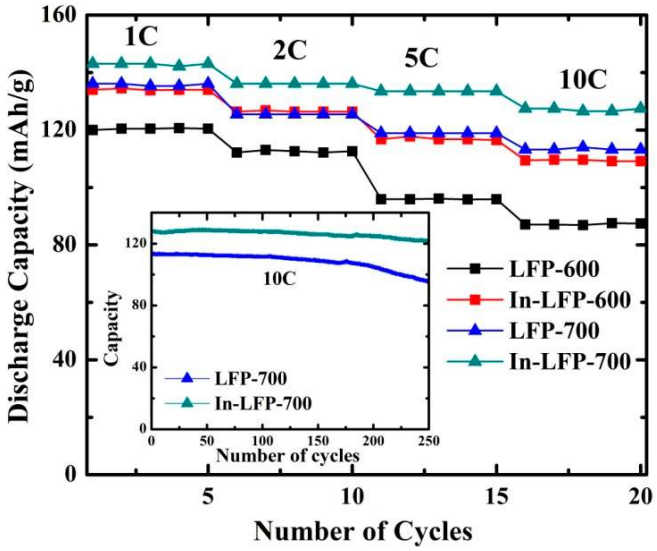

Figure 6. Rate capability curves of LFP-600, In-LFP-600, LFP-700, and In-LFP-700 samples during continuous cycling at different charging rates. The inset shows the capacity retention for LFP-700 and In-LFP-700 sample at 10 C rate.

Electrical impedance spectroscopy (EIS) measurements were also performed to understand the effects of In-doping on electrode impedance. The impedance spectra (Nyquist plots) of un-doped and In-doped $LiFePO_4$ samples are shown in Figure 7a are characteristic of electrochemical cells. The initial intercept of the semi-circle at highest frequency indicates resistance (R_s) associated to the electrolyte. The intercept of the semicircle in the intermediate frequency region corresponds to the charge transfer resistance (R_{ct}) in the bulk of electrode material, and the inclined line in the low frequency range represents the Warburg resistance (R_w), which is associated with lithium-ion diffusion. The data can be fitted to a Randles circuit (see insert in Figure 7a) in consisting of a constant phase element (CPE) representing the double layer capacitance and passivation film capacitance [34]. It has been observed that R_s values for the cells are very close to each other because the same electrolyte (1M $LiPF_6$ in EC/DMC 50:50 solvent) is used in all the cells. On the other hand, R_{ct} is lower in case of In-doped samples compared to the pure samples. This lower impedance of the In-doped sample may help to overcome the kinetic activation over potential for the Fe^{2+}/Fe^{3+} redox reaction during the charge–discharge process, and improve the capacity and cycling performance of the material.

We have determined the diffusion coefficient of lithium ion (D_{Li}) by using Z' dependence on ω in the low frequency region, which is described by [35],

$$Z' = R_s + R_{ct} + \sigma\omega^{-1/2} \quad (2)$$

where, σ is the Warburg coefficient, R_s and R_{ct} are the solution and the charge transfer resistances. σ is related to D_{Li} by

$$D_{Li} = R^2T^2/2A^2n^4F^4C_{Li}^2\sigma^2 \quad (3)$$

where, R is the gas constant, T is the temperature in Kelvins, n is the number of electrons per molecule during oxidation, A is the surface area of the cathode (0.28 cm^2 in our case), F is the Faraday constant, and C_{Li} is the concentration of lithium ion (0.0228 mol/cm^3 in this case). As expected, a plot of Z' vesus $\omega^{-1/2}$ shows (Figure 7b) a linear relationship which yields σ. An apparent exchange current density (I_o) [35], has been calculated to measure the enhanced reaction rate of electrodes, which is a measure of kinetics of an electrochemical reaction.

$$I_o = RT/nR_{ct}F \quad (4)$$

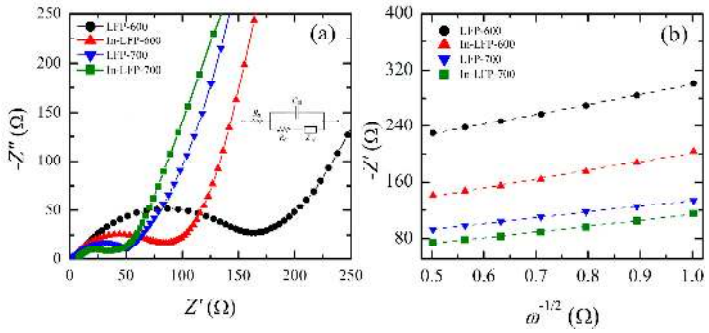

Figure 7. (**a**) Nyquist plots of LFP-600, In-LFP-600, LFP-700, and In-LFP-700 samples and (**b**) plot of the Z' vs. $\omega^{-1/2}$ in the low frequency region.

The calculated charge transfer resistance, lithium diffusion cofficent and apparent exchange current density along with other relevant parameters for the samples are given in Table 4. Indium doped $LiFePO_4/C$ samples have a lower charge transfer resistance of 77 Ω and 32 Ω for the In-LFP-600 and In-LFP-700 samples compared to 158 Ω and 72 Ω for the un-doped LFP-600 and LFP-700 samples. There is no drastic improvement in the lithium diffusion coefficient with In doping. However, lithium diffusion coefficient for In-LFP-700 is about a factor of two higher than the In-LFP-600 sample thus implying that annealing at 700 °C is desirable to improve the electrochemical properties of this material. Overall, the electrochemical measurements show that In-LFP-700 has the least charge transfer resistance, relatively higher Li-ion diffusion coefficient, and large exchange current density, which are consistent with its superior electrochemical performance in terms capacity and cycleability.

Table 4. Charge transfer resistance, Lithium diffusion coefficient, and exchange current density LFP-600 and LFP-700 compared with In-LFP-600 and In-LFP-700 samples.

Sample	R_{ct} (Ω)	σ (Ω $s^{1/2}$)	D_{Li} ($cm^2 \cdot s^{-1}$)	I_o ($mA \cdot g^{-1}$)
LFP-600 *	158	142	4.5×10^{-14}	163
In-LFP-600	77	124	6.0×10^{-14}	334
LFP-700 *	52	83	1.3×10^{-13}	494
In-LFP-700	32	82	1.4×10^{-13}	802

* see reference [27].

3. Materials and Methods

3.1. Synthesis Procedure

In-doped $LiFePO_4$/C samples were prepared by sol–gel technique, using $CH_3CO_2Li{\cdot}2H_2O$, $FeCl_2{\cdot}4H_2O$, P_2O_5 and $InCl_3$ as starting raw materials. These chemicals were mixed in stoichiometric ratio in dry ethanol and stirred for three hours, followed by the addition of 0.75 M lauric acid as carbon source to the mixture. After three hours of mixing the sol was dried under atmospheric conditions. The In-doped-$LiFePO_4$/C sample was prepared by adding 1 mol % of $InCl_3$ during the first step so that Fe:In ratio remains 99:1. The dried powders were ground and annealed under reduced environment of H_2 (10%) and Ar (90%) for 10 h. Two temperatures, 600 °C and 700 °C, were used to investigate the effects of annealing temperature with heating and cooling rate of 1 °C/min. In what follows, In-doped-$LiFePO_4$/C samples annealed at 600 °C and 700 °C will be referred as In-LFP-600, and In-LFP-700. The un-doped $LiFePO_4$ samples annealed at 600 °C and 700 °C, investigated in our previous study [27] will be referred as LFP-600 and LFP-700.

3.2. Characterization

Powder X-ray diffraction (XRD) patterns were obtained with a Rigaku Minflex-600 diffractometer (Osaka, Japan) using Cu Kα (λ = 1.54 Å) X-rays. Carbon content of the samples was measured by CHN analyzer, and found to be ~4.5%. The room temperature conductivity of the sample pellets were measured using 4-probe Van der Pauw method. The morphology of the samples was investigated using a JSM-6510-LV-LGS scanning electron microscope (SEM) (Tokyo, Japan) and a JEOL 2010 transmission microscope (TEM) (Tokyo, Japan). ^{57}Fe Mössbauer spectra were measured and fitted to obtain Mössbauer parameters using equipment and procedure described in our earlier work [36]. XPS measurements were performed using a Perkin-Elmer XPS systems (Waltham, UK), equipped with a cylindrical mirror analyzer and a highly monochromatic Al Kα (1486.6 eV) X-ray source. The observed binding energies of each element were identified with Perkin-Elmer database and an internal carbon source.

3.3. Electrochemical Measurements

The electrochemical characterization of the samples was performed in a standard coin cell geometry, using a Gamry electrochemical measurement system, in the frequency range of 0.1 Hz–100 kHz with an ac amplitude of 10 mV, as described in Ref. [12].

4. Conclusions

In (1 mol %)-doped-C-$LiFePO_4$ samples were prepared successfully by sol–gel method using lauric acid as surfactant to coat the particles under high temperature (600–700 °C) annealing. The carbon supplied by the decomposition of fatty acid not only provides reducing environment for maintaining Fe^{2+} in the $LiFePO_4$, but also restricts the growth of particle size of $LiFePO_4$. The XRD patterns of the samples indicates that In-doping does not affect the olivine crystal structure of $LiFePO_4$/C nanocomposites, but affects the amount of minority impurity phases (Fe_2P and Li_3PO_4) formed due to decomposition $LiFePO_4$ at higher annealing temperatures under a reducing environment. The presence of Fe_2P in the samples significantly enhances the electronic conductivity and hence affects its electrochemical properties. Of all the samples studied (doped and un-doped), we found that the In-doped-$LiFePO_4$/C nanocomposite annealed at 700 °C, containing 11 wt % Fe_2P showed the highest specific discharge capacity of ~142 mAh·g^{-1} at 1 C, ~128 mAh·g^{-1} at 10 C rate with a retention of 96% after 250 cycles of charging/discharging. However, our results demonstrate that by combining In-doping with high temperature (700 $\pm$ 50 °C) annealing, the electrochemical performance of $LiFePO_4$/C can be further improved by optimizing the amount of Fe_2P in the nanocomposites for good electronic conductivity without sacrificing the active material. It is important to note that carbon coating alone would not enhance the performance of $LiFePO_4$, but simultaneous indium doping

and carbon coating is a feasible way to improve electrochemical performance of $LiFePO_4$ for high power applications.

Acknowledgments: We thank the Richard Barber Foundation for financial support for this work.

Author Contributions: Gholam-Abbas Nazri, Ratna Naik, Vaman M. Naik, and Zhixian Zhou conceived and supervised the project and wrote the manuscript. Ajay Kumar, Parisa Bashiri, Balaji P. Mandal, Kulwinder S. Dhindsa, Khadije Bazzi synthesized the materials and did the XRD, SEM, TEM and electrochemical characterization and analysis. Maryam Nazri helped in the fabrication of coin cells, and Ambesh Dixit did the XPS measurements and analysis. Vijayendra K. Garg, Aderbal C. Oliveira, and Prem P. Vaishnava did the Mössbauer measurements and analyses.

Conflicts of Interest: The authors declare no conflict of interest.

References

1. Padhi, A.K.; Nanjundaswamy, K.S.; Goodenough, J.B. Phospho-olivines as Positive-Electrode Materials for Rechargeable Lithium Batteries. *J. Electrochem. Soc.* **1997**, *144*, 1188–1194. [CrossRef]
2. Lim, S.; Yoon, C.S.; Cho, J. Synthesis of nanowire and hollow $LiFePO_4$ cathodes for high-performance lithium batteries. *Chem. Mater.* **2008**, *20*, 4560–4564. [CrossRef]
3. Delmas, C.; Maccario, M.; Croguennec, L.; Cras, F.L.; Weill, F. Lithium deintercalation in $LiFePO_4$ nanoparticles via a domino-cascade model. *Nat. Mater.* **2008**, *7*, 665–671. [CrossRef] [PubMed]
4. Gibot, P.; Casas-Cabanas, M.; Laffont, L.; Levasseur, S.; Carlach, P.; Hamelet, S.; Tarascon, J.-M.; Masquelier, C. Room-temperature single-phase Li insertion/extraction in nanoscale Li_xFePO_4. *Nat. Mater.* **2008**, *7*, 741–747. [CrossRef] [PubMed]
5. Hsu, K.-F.; Tsay, S.-Y.; Hwang, B.-J. Synthesis and characterization of nano-sized $LiFePO_4$ cathode materials prepared by a citric acid-based sol–gel route. *J. Mater. Chem.* **2004**, *14*, 2690–2695. [CrossRef]
6. Huang, Y.-H.; Goodenough, J.B. High-Rate $LiFePO_4$ Lithium Rechargeable Battery Promoted by Electrochemically Active Polymers. *Chem. Mater.* **2008**, *20*, 7237–7241. [CrossRef]
7. Chen, Z.; Dahn, J.R. Reducing carbon in $LiFePO_4$/C composite electrodes to maximize specific energy, volumetric energy, and tap density. *J. Electrochem. Soc.* **2002**, *149*, A1184–A1189. [CrossRef]
8. Doeff, M.M.; Wilcox, J.D.; Kostecki, R.; Lau, G. Optimization of carbon coatings on $LiFePO_4$. *J. Power Sources* **2006**, *163*, 180–184. [CrossRef]
9. Dominko, R.; Bele, M.; Gaberscek, M.; Remskar, M.; Hanzel, D.; Pejovnik, S.; Jamnik, J. Impact of the Carbon coating thickness on the electrochemical performance of $LiFePO_4$/C composites. *J. Electrochem. Soc.* **2005**, *152*, A607–A610. [CrossRef]
10. Dominko, R.; Bele, M.; Goupil, J.-M.; Gaberscek, M.; Hanzel, D.; Arcon, I.; Jamnik, J. Wired porous cathode materials: A novel concept for synthesis of $LiFePO_4$. *Chem. Mater.* **2007**, *19*, 2960–2969. [CrossRef]
11. Huang, H.; Yin, S.-C.; Nazar, L.F. Approaching theoretical capacity of $LiFePO_4$ at room temperature at high rates. *Electrochem. Solid State Lett.* **2001**, *4*, A170–A172. [CrossRef]
12. Bazzi, K.; Mandal, B.P.; Nazri, M.; Naik, V.M.; Garg, V.K.; Oliveira, A.C.; Vaishnava, P.P.; Nazri, G.A.; Naik, R. Effect of Surfactants on the Electrochemical Behavior of $LiFePO_4$ Cathode Material for Lithium Ion Batteries. *J. Power Sources* **2014**, *265*, 67–74. [CrossRef]
13. Wagemaker, M.; Ellis, B.L.; Lützenkirchen-Hecht, D.; Mulder, F.M.; Nazar, L.F. Proof of Supervalent Doping in Olivine $LiFePO_4$. *Chem. Mater.* **2008**, *20*, 6313–6315. [CrossRef]
14. Ou, X.; Liang, G.; Wang, L.; Xu, S.; Zhao, X. Effect of Magnesium doping on electronic conductivity and electrochemical properties of $LiFePO_4$. *J. Power Sources* **2008**, *184*, 543–547. [CrossRef]
15. Yin, X.; Huang, K.; Liu, S.; Wang, H.; Wang, H. Preparation and characterization of Na-doped $LiFePO_4$/C composites as cathode materials for lithium-ion batteries. *J. Power Sources* **2010**, *195*, 4308–4312. [CrossRef]
16. Pang, L.; Zhao, M.; Zhao, X.; Chai, Y. Preparation and electrochemical performance of Gd-doped $LiFePO_4$/C composites. *J. Power Sources* **2012**, *201*, 253–258. [CrossRef]
17. Zhao, X.; Tang, X.; Zhang, L.; Zhao, M.; Zhai, J. Effects of neodymium aliovalent substitution on the structure and electrochemical performance of $LiFePO_4$. *Electrochim. Acta* **2010**, *55*, 5899–5904. [CrossRef]
18. Cho, Y.-D.; Fey, G.T.-K.; Kao, H.-M. Physical and electrochemical properties of La-doped $LiFePO_4$/C composites as cathode materials for lithium-ion batteries. *J. Solid State Electrochem.* **2008**, *12*, 815–823. [CrossRef]

19. Chung, S.-Y.; Bloking, J.T.; Chiang, Y.-M. Electronically conductive phospho-olivines as lithium storage electrodes. *Nat. Mater.* **2002**, *1*, 123–128. [CrossRef] [PubMed]
20. Islam, M.S.; Driscoll, D.J.; Fisher, C.A.; Slater, P.R. Atomic-Scale Investigation of Defects, Dopants, and Lithium Transport in the $LiFePO_4$ Olivine-Type Battery Material. *Chem. Mater.* **2005**, *17*, 5085–5092. [CrossRef]
21. Kim, C.W.; Park, J.S.; Lee, K.S. Effect of Fe_2P on the electron conductivity and electrochemical performance of $LiFePO_4$ synthesized by mechanical alloying using Fe^{3+} raw material. *J. Power Sources* **2006**, *163*, 144–150. [CrossRef]
22. Qiu, Y.; Geng, Y.; Yu, J.; Zuo, X. High-capacity cathode for lithium-ion battery from $LiFePO_4$/(C + Fe_2P) composite nanofibers by electrospinning. *J. Mater. Sci.* **2014**, *49*, 504–509. [CrossRef]
23. Xu, Y.; Lu, Y.; Yan, L.; Yang, Z.; Yang, R. Synthesis and effect of forming Fe_2P phase on the physics and electrochemical properties of $LiFePO_4$/C materials. *J. Power Sources* **2006**, *160*, 570–576. [CrossRef]
24. Herle, P.S.; Ellis, B.; Coombs, N.; Nazar, L.F. Nano-network electronic conduction in iron and nickel olivine phosphates. *Nat. Mater.* **2004**, *3*, 143–152. [CrossRef] [PubMed]
25. Rho, Y.-H.; Nazar, L.F.; Perry, L.; Ryan, D. Surface Chemistry of $LiFePO_4$ Studied by Mössbauer and X-ray Photoelectron Spectroscopy and Its Effect on Electrochemical Properties. *J. Electrochem. Soc.* **2007**, *154*, A283–A289. [CrossRef]
26. Lin, Y.; Gao, M.; Zhu, D.; Liu, Y.; Pan, H. Effects of carbon coating and iron phosphides on the electrochemical properties of $LiFePO_4$/C. *J. Power Sources* **2008**, *184*, 444–448. [CrossRef]
27. Dhindsa, K.; Kumar, A.; Nazri, G.; Naik, V.; Garg, V.; Oliveira, A.; Vaishnava, P.; Zhou, Z.; Naik, R. Enhanced electrochemical performance of $LiFePO_4$/C nanocomposites due to in situ formation of Fe_2P impurities. *J. Solid State Electrochem.* **2016**, *20*, 2275–2282. [CrossRef]
28. Kang, B.; Ceder, G. Battery materials for ultrafast charging and discharging. *Nature* **2009**, *458*, 190–193. [CrossRef] [PubMed]
29. Castro, L.; Dedryvere, R.; El Khalifi, M.; Lippens, P.-E.; Bréger, J.; Tessier, C.; Gonbeau, D. The Spin-Polarized Electronic Structure of $LiFePO_4$ and $FePO_4$ Evidenced by in-Lab XPS. *J. Phys. Chem. C* **2010**, *114*, 17995–18000. [CrossRef]
30. Castro, L.; Dedryvère, R.; Ledeuil, J.-B.; Bréger, J.; Tessier, C.; Gonbeau, D. Aging Mechanisms of $LiFePO_4$//Graphite Cells Studied by XPS: Redox Reaction and Electrode/Electrolyte Interfaces. *J. Electrochem. Soc.* **2012**, *159*, A357–A363. [CrossRef]
31. Yamada, A.; Chung, S.-C.; Hinokuma, K. Optimized $LiFePO_4$ for Lithium Battery Cathodes. *J. Electrochem. Soc.* **2001**, *148*, A224–A229. [CrossRef]
32. Prince, A.; Mylswamy, S.; Chan, T.; Liu, R.; Hannoyer, B.; Jean, M.; Shen, C.; Huang, S.; Lee, J.; Wang, G. Investigation of Fe valence in $LiFePO_4$ by Mössbauer and XANES spectroscopic techniques. *Solid State Commun.* **2004**, *132*, 455–458. [CrossRef]
33. Liu, Y.; Cao, C.; Li, J. Enhanced electrochemical performance of carbon nanospheres–$LiFePO_4$ composite by PEG based sol–gel synthesis. *Electrochim. Acta* **2010**, *55*, 3921–3926. [CrossRef]
34. Wang, G.; Yang, L.; Chen, Y.; Wang, J.; Bewlay, S.; Liu, H. An investigation of polypyrrole-$LiFePO_4$ composite cathode materials for lithium-ion batteries. *Electrochim. Acta* **2005**, *50*, 4649–4654. [CrossRef]
35. Bard, A.J.; Faulkner, L.R.; Leddy, J.; Zoski, C.G. *Electrochemical Methods: Fundamentals and Applications*; Wiley: New York, NY, USA, 1980; Volume 2.
36. Dhindsa, K.; Mandal, B.P.; Bazzi, K.; Lin, M.; Nazri, M.; Nazri, G.; Naik, V.; Garg, V.; Oliveira, A.; Vaishnava, P.; et al. Enhanced electrochemical performance of graphene modified $LiFePO_4$ cathode material for lithium ion batteries. *Solid State Ion.* **2013**, *253*, 94–100. [CrossRef]